Identification and Characterization of a Bacterial Glycerol-1-phosphate Dehydrogenase: Ni^{2+}-Dependent AraM from *Bacillus subtilis*†

Harald Guldan, Reinhard Sterner, and Patrick Babinger*

Institute of Biophysics and Physical Biochemistry, University of Regensburg, Universitätsstrasse 31, D-93053 Regensburg, Germany

Received April 3, 2008; Revised Manuscript Received May 9, 2008

ABSTRACT: The exclusive presence of glycerol-1-phosphate dehydrogenases (G1PDH) has been postulated to be a key feature that distinguishes archaea from bacteria. However, homologues of G1PDH genes can be found in several bacterial species, among them the hitherto uncharacterized open reading frame *araM* from *Bacillus subtilis*. We produced recombinant AraM in *Escherichia coli* and demonstrate that the purified protein forms a homodimer that reversibly reduces dihydroxyacetone phosphate (DHAP) to glycerol-1-phosphate (G1P) in a NADH-dependent manner. AraM, which constitutes the first identified G1PDH from bacteria, has a similar catalytic efficiency as its archaeal homologues, but its activity is dependent on the presence of Ni^{2+} instead of Zn^{2+}. On the basis of these findings and the analysis of an *araM* knockout mutant, we propose that AraM generates G1P for the synthesis of phosphoglycerolipids in Gram-positive bacterial species.

On the basis of 16S rRNA comparisons, the phylogentic tree of life has been divided into the three domains of bacteria, archaea, and eucarya (*1*). The nature of the last common ancestor and the molecular events leading to the divergence into the three domains are a matter of controversial discussion. Many scientists link the segregation between archaea and bacteria to the evolution of their different membrane compositions (*2, 3*). Briefly, the core of a bacterial or eukaryotic phospholipid is a *sn*-glycerol-3-phosphate (G3P),[1] to which two fatty acids are bound through an ester linkage. In contrast, the archaeal phospholipid contains isoprenoid derivatives instead of fatty acids, which are linked to *sn*-glycerol-1-phosphate (G1P) via an ether bond. Consequently, the emergence of domain-specific key enzymes for phospholipid biosynthesis like the archaeal geranylgeranylglyceryl phosphate synthase (GGGPS; *4, 5*) or stereospecific glycerol-phosphate dehydrogenases (*3, 6*) producing G1P (G1PDH) and G3P (G3PDH), respectively (*7–9*), have been regarded as cornerstones of the differentiation between archaea and bacteria/eucarya.

Since G1PDHs have been identified only in archaea, free G1P was assumed not to exist in species of the other two phylogenetic domains. In bacteria, however, G1P has been found in bound form as a component of the lipoteichoic acids (LTA) of Gram-positives (*10, 11*), in phosphatidylglycerols (*12*), and in the lipopolysaccharide (LPS; *13*). But as far as it is known, in all of these molecules the G1P moiety is produced from alternate substrates, e.g., by changing the stereoisomery from G3P to G1P in case of LTA biosynthesis. Nevertheless, we asked whether there could be a G1P-producing enzyme in bacteria being involved in the biosynthetic pathways that produce those components.

To identify such enzymes, we performed a BLAST search with the G1PDH sequence from *Archaeoglobus fulgidus* (EgsA) and found that the AraM protein of *Bacillus subtilis* displays 31% sequence identity to the query. The *araM* gene is a member of the *B. subtilis* arabinose operon, but its function has remained unknown until now (*14*). We then produced AraM in *Escherichia coli*, purified the recombinant protein, and characterized it by hydrodynamic measurements and ligand titration studies as well as steady-state enzyme kinetics. The results show that *B. subtilis* AraM is a homodimer, which constitutes the first known G1PDH from bacteria. It binds its coenzyme NADH with high affinity and is dependent on Ni^{2+} instead of Zn^{2+}, which is the metal cofactor of archaeal G1PDHs. The G1PDH activity of AraM was demonstrated *in vivo* by analyzing a knockout mutant. On the basis of the obtained results, we propose that AraM generates G1P to be used by the PcrB enzyme for the synthesis of phosphoglycerolipids in Gram-positive bacteria.

EXPERIMENTAL PROCEDURES

Cloning and Expression of the araM Gene and Purification of the Recombinant Protein. The *araM* gene from *B. subtilis* subsp. *subtilis* str. 168 was amplified by PCR from genomic DNA and cloned into the *Nde*I and *Xho*I sites of the

† This work was supported by the University of Regensburg and a fellowship of the Konrad-Adenauer-Stiftung to H.G.

* Corresponding author. Phone: +49 (941) 943 1634. Fax: +49 (941) 943 2813. E-mail: patrick.babinger@biologie.uni-r.de.

[1] Abbreviations: DHAP, dihydroxyacetone phosphate; ESI-MS, electrospray ionization mass spectrometry; FRET, fluorescence resonance energy transfer; GGGPS, geranylgeranylglyceryl phosphate synthase; G1P, *sn*-glycerol-1-phosphate; G3P, *sn*-glycerol-3-phosphate; G1PDH, glycerol-1-phosphate dehydrogenase; G3PDH, glycerol-3-phosphate dehydrogenase; GGPP, geranylgeranyl pyrophosphate; HGT, horizontal gene transfer; HRP, horseradish peroxidase; ICP-OES, inductively coupled plasma optical emission spectrometry; IPTG, isopropyl β-D-1-thiogalactopyranoside; LPS, lipopolysaccharide; LTA, lipoteichoic acid.

10.1021/bi8005779 CCC: $40.75
Published on Web 06/18/2008

expression vector pET-21a (Novagen; C-terminal His_6 tag added to the recombinant protein). Inadvertent mutations of the cloned gene were excluded by DNA sequencing. Heterologous expression of the gene was performed in *E. coli* BL21(DE3) cells (Stratagene) transformed with the plasmid construct. The cells were grown at 37 °C in LB medium containing 150 μg/mL ampicillin. After an OD_{600} of 0.6−0.8 was reached, expression was induced with 0.5 mM isopropyl β-D-1-thiogalactopyranoside (IPTG), and growth was continued until the culture reached its stationary phase. In order to obtain fully active AraM, the medium was supplemented with 25 mM potassium phosphate, pH 8.0, containing 1 mM $NiCl_2$ (see Results and Discussion section). Cells were harvested by centrifugation (Sorvall 5C plus, GS3, 30 min, 4 °C), resuspended in 100 mM potassium phosphate, pH 8.0, containing 300 mM KCl and 10 mM imidazole, and disrupted by ultrasonication. Following centrifugation (Sorvall 5C plus, SS34, 60 min, 4 °C), the supernatant containing the soluble cell extract was loaded onto a Ni^{2+}-chelate affinity column (HisTrap Crude FF, 5 mL; GE Healthcare). Bound proteins were eluted at room temperature with a linear gradient from 10 to 500 mM imidazole dissolved in 100 mM potassium phosphate, pH 8.0, containing 300 mM KCl. Recombinant AraM purified from an expression culture grown without supplemented Ni^{2+} showed no activity, indicating that there is no metal released from the column during chromatography. The AraM preparations were pure to at least 95%, as judged by SDS−PAGE.

Following dialysis against 50 mM potassium phosphate, pH 8.0 at 4 °C, the concentration of purified AraM was determined by absorbance spectroscopy. To this end a molar extinction coefficient at 280 nm of 28670 M^{-1} cm^{-1} was used, which was calculated from the amino acid sequence (*15*). About 45 mg of AraM were obtained from 1 L of growth medium. Purified protein was dropped into liquid nitrogen and stored at −80 °C.

Analytical Methods. The calculated molecular mass of the AraM polypeptide chain was verified by electrospray ionization mass spectrometry (ESI-MS). ESI-MS and fragmentation were performed by using an Ion Trap ESQUIRE LC instrument (Bruker, Billerica, MA). Samples were infused by a nanospray source in MeOH (50%)/AcOH (0.5%). The association state of purified AraM was determined at room temperature by analytical gel filtration and analytical ultracentrifugation. Analytical gel filtration was done using a calibrated Superdex 75 column (1 cm × 30 cm; GE Healthcare) that was equilibrated with 50 mM potassium phosphate, pH 8.0, containing 300 mM KCl. AraM (100 μL with a subunit concentration of 22 μM) was applied to the column and eluted at 25 °C with a flow rate of 0.5 mL/min, following the absorbance at 280 nm. Sedimentation equilibrium runs were performed at 26 °C using a Beckman ultracentrifuge (Model E) at 16000 or 12000 rpm with an An-G rotor containing 12 mm double sector cells filled with 10 μM (subunit concentration) AraM dissolved in 100 mM Tris-HCl, pH 7.5, and followed by measuring the absorbance at 277 nm. The runs were analyzed using the meniscus-depletion-sedimentation-equilibrium method (*16*). Molecular masses were calculated assuming a partial specific volume of 0.739 mL/g, as calculated from the AraM amino acid sequence (*17, 18*).

Absorbance and far-UV circular dichroism spectra of AraM were recorded at 25 °C, using a Cary 100 spectrometer (Varian) (d = 1 cm) and an Aviv 62DS spectrophotometer (Aviv Biomedical Inc.) (d = 0.1 cm), respectively. Fluorescence studies were carried out at 25 °C using a Cary Eclipse spectrometer (Varian) (d = 1 cm). Excitation spectra of NADH were collected from 250 to 400 nm. Emission spectra were recorded by exciting the NADH fluorescence at 340 nm and measuring the fluorescence intensity from 350 to 650 nm.

Steady-State Enzyme Kinetics. Prior to activity measurements, AraM was rebuffered from 50 mM potassium phosphate into 50 mM Tris-HCl, pH 8.8 at 25 °C (corresponding to pH 8.2 at 45 °C), in order to avoid competitive inhibition of substrate binding by residual ortho-phosphate. The reduction of DHAP to G1P was measured at 45 °C by following the absorbance decrease at 340 nm, which is caused by the concomitant oxidation of NADH to $NAD^+ + H^+$. The reaction mixture contained 50 mM Tris-HCl, pH 8.2 and 1 μM (subunit concentration) of AraM. The pH optimum of AraM was determined at 45 °C in the following buffers: MES (pH 5.6−6.8), MOPS (pH 6.4−7.6), HEPES (pH 6.9−7.7), and Tris-HCl (pH 6.4−9.0). The pH values of all buffers were titrated at 25 °C such that the desired values were reached at 45 °C, using published $\Delta pK_a/\Delta T$ data (*19*). To determine the Michaelis constants (K_M) and turnover numbers (k_{cat}), one substrate was offered at saturating concentrations (>10K_M: 0.1 mM DHAP; 0.25 mM NADH; 10 mM G1P; 4 mM NAD^+), and the concentration of the second substrate was varied. The resulting saturation curves were fitted to the Michaelis−Menten equation with a hyperbolic function (SigmaPlot 9.0), yielding values for the maximal velocity V_{max} and for K_M. The k_{cat} values were determined by dividing V_{max} by the subunit concentration of AraM ([E_0]). The catalytic efficiencies k_{cat}/K_M for DHAP, G1P, NADH, and NAD^+ were calculated by dividing the turnover numbers by the Michaelis constants. When NADPH was used instead of NADH, its K_M value was too high to reach saturation. Therefore, only k_{cat}/K_M^{NADPH} could be calculated from the slope of the linear part of the saturation curve, where [NADPH] ≪ K_M^{NADPH}.

NADH Titration. Titration of 0.5 μM AraM (subunit concentration) with NADH was followed by fluorescence resonance energy transfer (FRET) in 10 mM Tris-HCl, pH 8.0, at 25 °C. Following each titration step, the fluorescence of the AraM tryptophan residues was excited at 285 nm, and the emission of the protein−NADH mixture was followed between 300 and 450 nm. After equilibration, which took several minutes, binding was analyzed using the increase of NADH fluorescence intensity. To calculate the thermodynamic dissociation K_D^{NADH}, the fluorescence intensity was plotted against the concentration of total ligand. Data points were fitted (SigmaPlot 9.0) with the equation

$$F = F_0 + (F_{max} - F_0) \times 0.5[(1 + (L_0 + K_D^{NADH})/E_0) - ((1 + (L_0 + K_D^{NADH})/E_0)^2 - 4L_0/E_0)^{0.5}]$$

where F is the measured fluorescence after each titration step, F_{max} is the maximum and F_0 is the minimum observed fluorescence, L_0 is the total ligand concentration, and E_0 is the total protein subunit concentration (*20*). Inner filtering effects were negligible, because the absorbance of NADH

at the highest used concentration (2 μM) and at the excitation wavelength of 285 nm was < 0.005.

Metal-Induced Reactivation of AraM. To remove bound metal ions, 100 μM (subunit concentration) purified AraM was dialyzed against 50 mM EDTA and 50 mM Tris-HCl, pH 8.0, for 5 h at 4 °C. EDTA was then removed by extensive dialysis against 50 mM Tris-HCl, pH 8.0. The resulting protein sample did not show any detectable residual G1PDH activity. Apo-AraM was incubated with different concentrations of several bivalent cations ($NiCl_2$, $ZnCl_2$, $CuCl_2$, $CaCl_2$, $MgCl_2$, $MnCl_2$, $CoCl_2$, $Cd(CH_3COO)_2$, and $FeCl_2$) for 1 h at 4 °C, followed by measuring its G1PDH activity in the presence of saturating concentrations of DHAP (0.1 mM) and NADH (0.25 mM).

ICP-OES Measurements To Quantify Protein-Bound Metal. Solutions containing purified AraM were dialyzed against 50 mM potassium phosphate, pH 8.0, supplemented with an equal volume of HCl (32%), and incubated at 75 °C for 20 min to hydrolyze the peptide bonds. The samples were analyzed with a JY-70 Plus inductively coupled plasma optical emission spectrometer (Jobin Yvon) that had been calibrated with appropriate Ni, Zn, and S standard solutions. The measured molar concentrations of Ni and Zn were then set in relation to the concentration of the protein, which was determined via ICP-OES quantification of the sulfur from cysteine and methionine residues. The metal and sulfur contents from the dialysis buffer were subtracted as background. Control experiments were performed to exclude that the detected metals were unspecifically bound via the His_6 tag fused to AraM for purification of the recombinant protein.

Generation of a B. subtilis araM Knockout Mutant. To analyze the *in vivo* relevance of AraM, we generated a *B. subtilis* 168 strain with an inactivated *araM* gene using the pMUTIN method (*21*). To this end, a part of the *araM* gene was PCR-amplified and cloned into the pMUTIN4 vector. *B. subtilis* 168 was then transformed with this construct to destroy the genomic *araM* by insertional mutagenesis. The successful disruption of *araM* was verified both by PCR and Southern hybridization.

Cultivation of B. subtilis Strains. To test *B. subtilis* 168 and the knockout strain for phenotypic effects, the cells were grown on different media. C medium (70 mM K_2HPO_4, 30 mM KH_2PO_4, 25 mM $(NH_4)_2SO_4$, 0.5 mM $MgSO_4$, 10 μM $MnSO_4$, 22 mg/L ferric ammonium citrate, 100 mg/L tryptophan) (*22*) was used as minimal medium. CSE medium is C minimal medium supplemented with sodium succinate (6 g/L) and potassium glutamate (8 g/L). C-Glc is C minimal medium supplemented with glucose (5 g/L).

LTA Analysis by ELISA. The contents of lipoteichoic acids in *B. subtilis* wild type (wt) and the *araM* knockout strain were quantified by ELISA. The experiment was carried out as described (*23*) with minor modifications. After the cells were grown for 5 h or overnight in LB medium, LTA were extracted from equal amounts of cells (as estimated from OD_{600}) and applied in dilution series to ELISA plates (10^{-1} to 2×10^{-3}). *E. coli* extracts were used as negative control. The monoclonal anti-LTA antibody, clone 55 (Dunn Labortechnik GmbH, Asbach, Germany; 1:150 dilution), reliably detected *B. subtilis* LTA and yielded no background in the controls. As secondary antibody we used an anti-mouse IgG from sheep linked to HRP (NA 931; GE Healthcare) with a 1:1000 dilution. Detection was done with TMB ELISA HRP substrate (Dunn Labortechnik GmbH, Asbach, Germany) for 15 min and was stopped by adding 50 μL of 1 M H_2SO_4. Subsequently, the absorbance at 450 nm was recorded.

RESULTS AND DISCUSSION

Identification of AraM as a Putative G1PDH. To identify putative bacterial homologues of archaeal G1PDHs, we performed a BLAST search (*24*) with the G1PDH protein sequence from *A. fulgidus* (EgsA; Genbank accession no. O28599) as query. Among the hits, we found the AraM protein of *B. subtilis*, which showed a 31% sequence identity in the best local alignment (*E*-value 8×10^{-22}), and several other high-scoring proteins annotated as "AraM-like". The *araM* gene is located within the arabinose operon of *B. subtilis*, but the encoded protein is dispensable for growth on arabinose (*14*). The presence of a G1PDH-related protein in bacteria has already been noticed (*7, 25*) but was explained as a rare occurrence caused by horizontal gene transfer (HGT). A BLAST search with AraM as query resulted in a few dozen hits of closely related proteins spread over several Gram-positive and Gram-negative bacterial orders. Although not contradicting the HGT origin theory, this rather broad occurrence suggests that AraM has a specific function in those species.

A multiple sequence alignment of *B. subtilis* AraM with some G1PDH representatives (Figure 1) showed that the overall identity of AraM to the G1PDHs is 21−24%, while the G1PDHs among one another are 33−53% identical. Moreover, the alignment revealed that all residues in G1PDH predicted to interact with the substrate DHAP, the coenzyme NADH, and the metal cofactor Zn (*7*) are also present in AraM. This finding suggested that AraM is a G1PDH. To test this hypothesis, we expressed the *B. subtilis araM* gene heterologously in *E. coli* and purified the recombinant protein to homogeneity by metal chelate affinity chromatography.

Recombinant AraM Is a Homodimer with High NADH Affinity. Mass spectroscopy showed that purified AraM with a His_6 tag has a molecular mass (MW) of 44118 Da, which is close to the calculated subunit MW of 44122 Da. The oligomerization state and the homogeneity of the protein were determined by analytical gel filtration and analytical ultracentrifugation. The protein eluted from a calibrated Superdex 75 gel filtration column as a sharp peak corresponding to a MW of 72 kDa. The ln c vs r^2 plot (*16*) of a sedimentation equilibrium analysis showed no deviation from linearity, indicating absence of polydispersity and yielding a MW of 80 kDa. We conclude that AraM forms a homodimer, but cannot exclude a rapid equilibrium with a minor monomeric fraction under the given experimental conditions. The G1PDH from *Aeropyrum pernix* also exists as a homodimer (*26*), while G1PDH from *Methanococcus thermoautotrophicum* has been reported to form an octamer (*27*).

We noticed that purified AraM displayed significant blue fluorescence, which was visible by eye when excited with a UV lamp ($\lambda = 366$ nm). Spectroscopic analysis revealed an absorption peak at 340 nm that appeared in addition to the typical protein peak around 280 nm caused by tryptophan and tyrosine residues (Figure 2A), suggesting that a considerable amount of bound NADH was copurified with AraM.

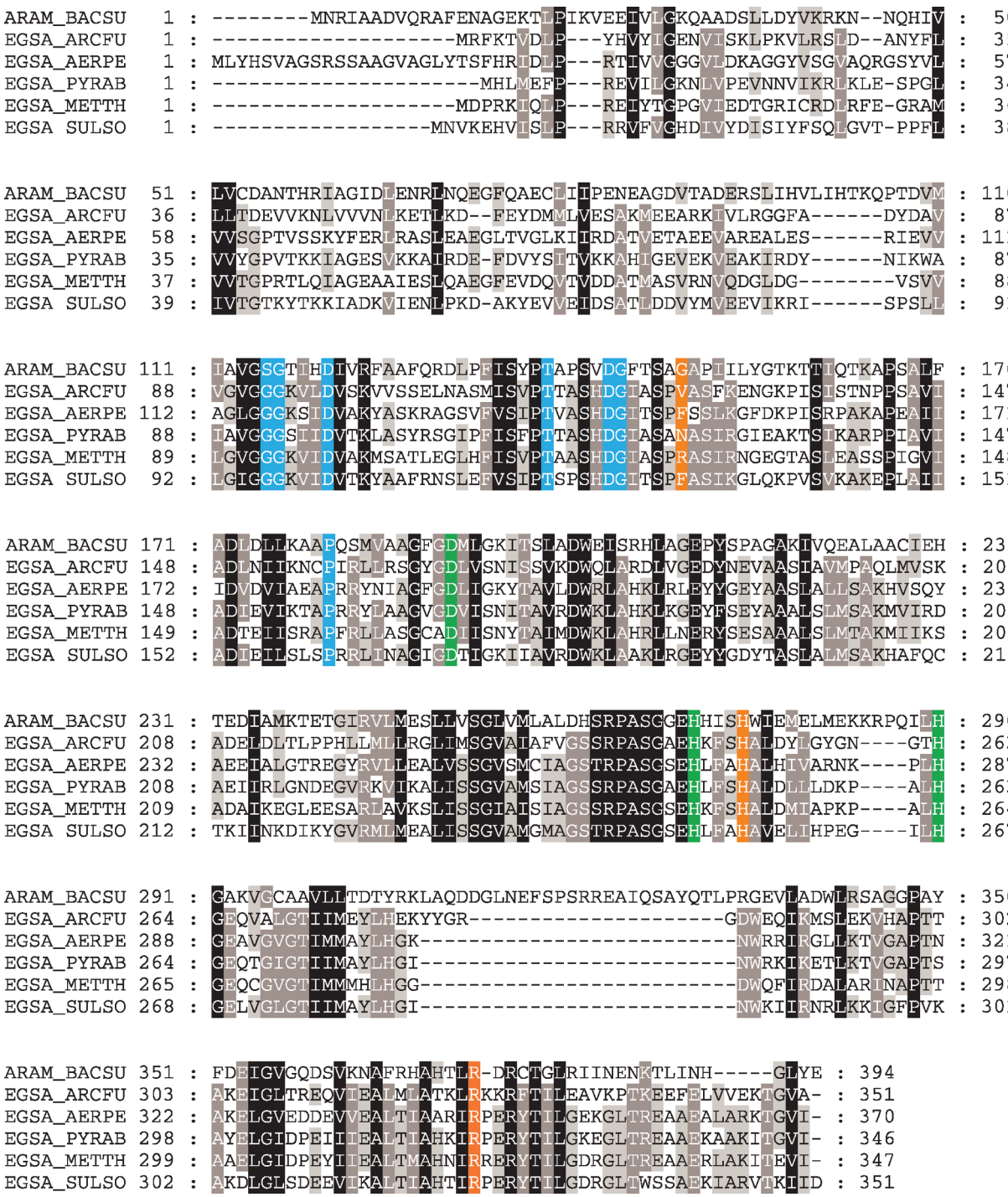

FIGURE 1: Multiple sequence alignment of several archaeal G1PDHs (EgsA) and *B. subtilis* AraM. The residues postulated to be involved in binding of substrate, coenzyme, and metal (*7*) are colored: orange, phosphate moiety of DHAP; blue, NADH; green, M^{2+}. Other residues are colored in different gray-to-black shadings with increasing degree of conservation. The sequences are named according to their Uniprot entries: *Bacillus subtilis* (ARAM_BACSU), *Archaeoglobus fulgidus* (EGSA_ARCFU), *Pyrococcus abyssi* (EGSA_PYRAB), *Aeropyrum pernix* (EGSA_AERPE), *Methanococcus thermoautotrophicus* (EGSA_METTH), and *Sulfolobus solfataricus* (EGSA_SULSO). The alignment was generated with T-COFFEE using standard settings.

When excited at 340 nm, the sample showed a fluorescence emission maximum at 425 nm (Figure 2B). The fluorescence maximum of free NADH lies at 465 nm, and its intensity is about 15-fold lower than that of the bound coenzyme. Similar differences between the fluorescence of free and protein-bound NADH have been reported previously (*28–30*) and have been ascribed to the more hydrophobic environment in the protein cofactor binding pocket compared to the bulk solvent (*31*). To further investigate the NADH binding characteristics of AraM, we added DHAP to convert bound NADH to NAD^+, which was then removed by dialysis. This reaction could be followed by eye using a UV lamp, where a loss of the blue fluorescence within a few seconds was observed. This finding suggested that AraM has G1PDH activity. The NADH binding to AraM was then quantified by titration measurements that were recorded by FRET (*30, 31*). To this end, the intrinsic tryptophan fluorescence of the protein was excited at 285 nm, and the emission of the

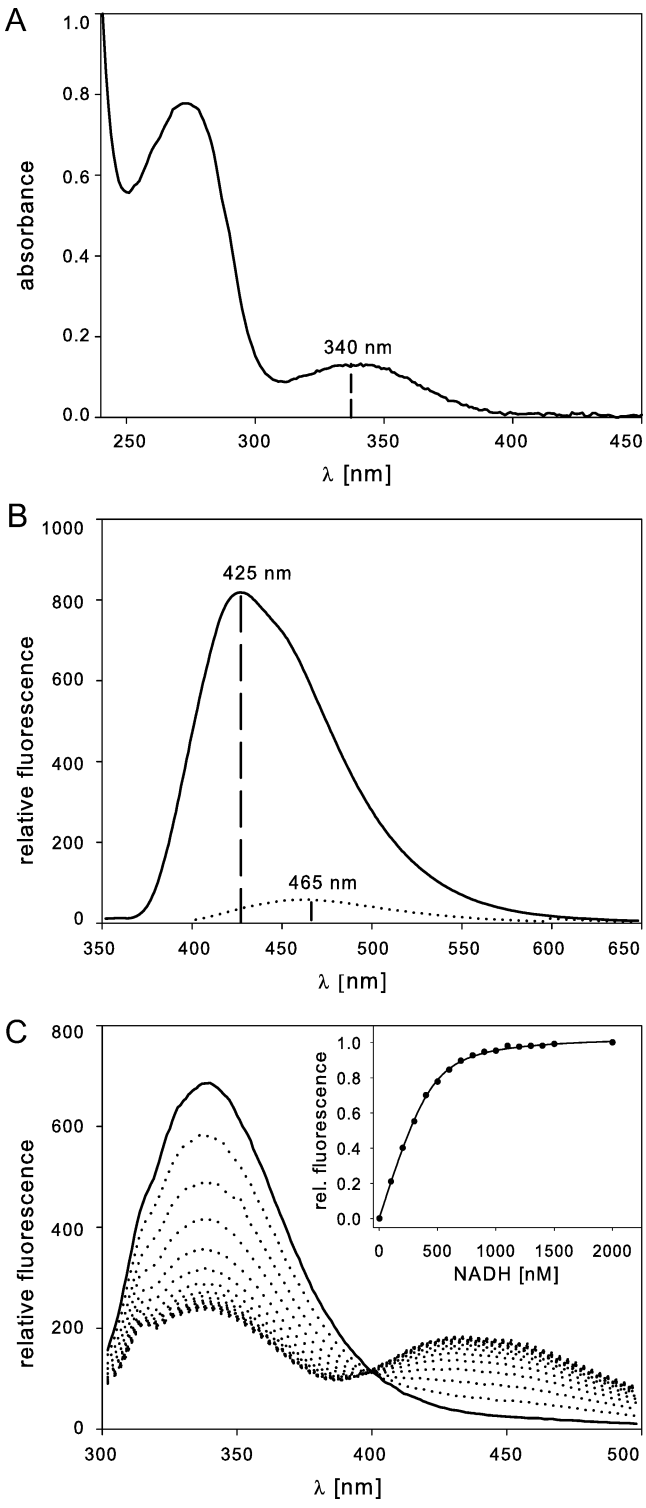

FIGURE 2: Spectroscopic characterization of NADH binding to AraM. (A) Absorbance spectrum of 45 μM (subunit concentration) purified AraM. The peak at 340 nm corresponds to 19 μM bound NADH. (B) Fluorescence emission spectrum (excitation at 340 nm) of the same protein sample as used in (A) (solid line). For comparison, the spectrum of 19 μM free NADH is shown (dotted line). (C) FRET analysis of NADH binding to AraM at a subunit concentration of 0.5 μM. AraM shows a typical tryptophan fluorescence emission spectrum when excited at 285 nm (solid line). Titration with NADH results in a decrease of the protein fluorescence and a concomitant increase of the NADH fluorescence (dotted lines). The FRET signal was analyzed at 425 nm, yielding the hyperbolic binding curve shown in the inset. The measurements were performed in 10 mM Tris-HCl, pH 8.0, at 25 °C.

NADH fluorescence at 425 nm was monitored (Figure 2C). Denaturation of the protein in 8 M urea resulted in the disappearance of the FRET signal, supporting that it is caused by energy transfer between a tryptophan residue and the neighbored coenzyme bound to the folded protein. The analysis of the FRET data yielded a hyperbolic titration curve, with no indication of cooperative NADH binding to the AraM homodimer (inset to Figure 2C). A fit of the curve with a quadratic equation (see Experimental Procedures section) yielded a 1:1 stoichiometry for binding and a value for the thermodynamic dissociation constant K_D^{NADH} of 53 $\pm$ 5 nM. Comparably high affinities for NADH binding are not common but have been observed for some other proteins (*30, 32*).

Steady-State Enzyme Kinetics Show That AraM Has High G1PDH Activity. In order to quantify the G1PDH activity of AraM at the physiological growth temperature of *B. subtilis*, steady-state kinetic measurements were performed at 45 °C in both directions of the reversible reaction (Figure 3A). The resulting saturation curves (Figure 3B−E) were analyzed with the Michaelis−Menten equation, and the deduced turnover numbers k_{cat}, Michaelis constants K_M, and catalytic efficiencies k_{cat}/K_M are listed in Table 1. AraM catalyzes the NADH-dependent reduction of DHAP (Figure 3B,D) and the NAD^+-dependent oxidation of G1P but not of G3P (Figure 3C,E). The stereospecificity of the enzyme was confirmed by product inhibition of the DHAP reduction reaction, which could be achieved with G1P but not with G3P (Supporting Information Figure 1). Instead of NADH the enzyme can also use NADPH, but with much lower efficiency (Figure 3D, Table 1), in accordance with what has been reported for archaeal G1PDHs (*26*). The pH dependence of the activity of AraM at 45 °C revealed a flat profile with an optimum around pH = 8.2 (data not shown).

The COG classification (*33*) ranks AraM in the cluster COG0371 ("glycerol dehydrogenase (GDH) and related enzymes"). In order to exclude the possibility that AraM is a GDH with G1PDH side activity, enzyme tests were performed with glycerol and dihydroxyacetone as substrates and NAD^+ and NADH as coenzymes. No GDH activity could be detected in the presence of an AraM subunit concentration of 1 μM, confirming that the enzyme is a G1PDH.

To our knowledge, the only detailed kinetic study of a G1PDH was done with the enzyme from the hyperthermophilic archaeon *A. pernix*, which was investigated at 65 °C (*26, 34*). Compared to these data, the k_{cat} values of AraM at 45 °C are about 1 order of magnitude lower, both for the forward and reverse direction. However, the K_M values for the substrates and coenzymes are a factor of 3−26 lower for AraM. As a consequence, at the applied temperatures the catalytic efficiencies of the two enzymes differ by less than 10-fold.

The Catalytic Activity of AraM Is Ni^{2+}-Dependent. All known archaeal G1PDHs, as well as the related GDHs, require Zn^{2+} for catalytic activity (*7, 34, 35*). The first hint that this might be different in the case of AraM was the observation that we initially could purify active protein only when using a metal chelate column that had been freshly labeled with Ni^{2+} ions. To test the metal requirement of AraM, production of the recombinant protein was then performed in the presence of different mixtures of bivalent

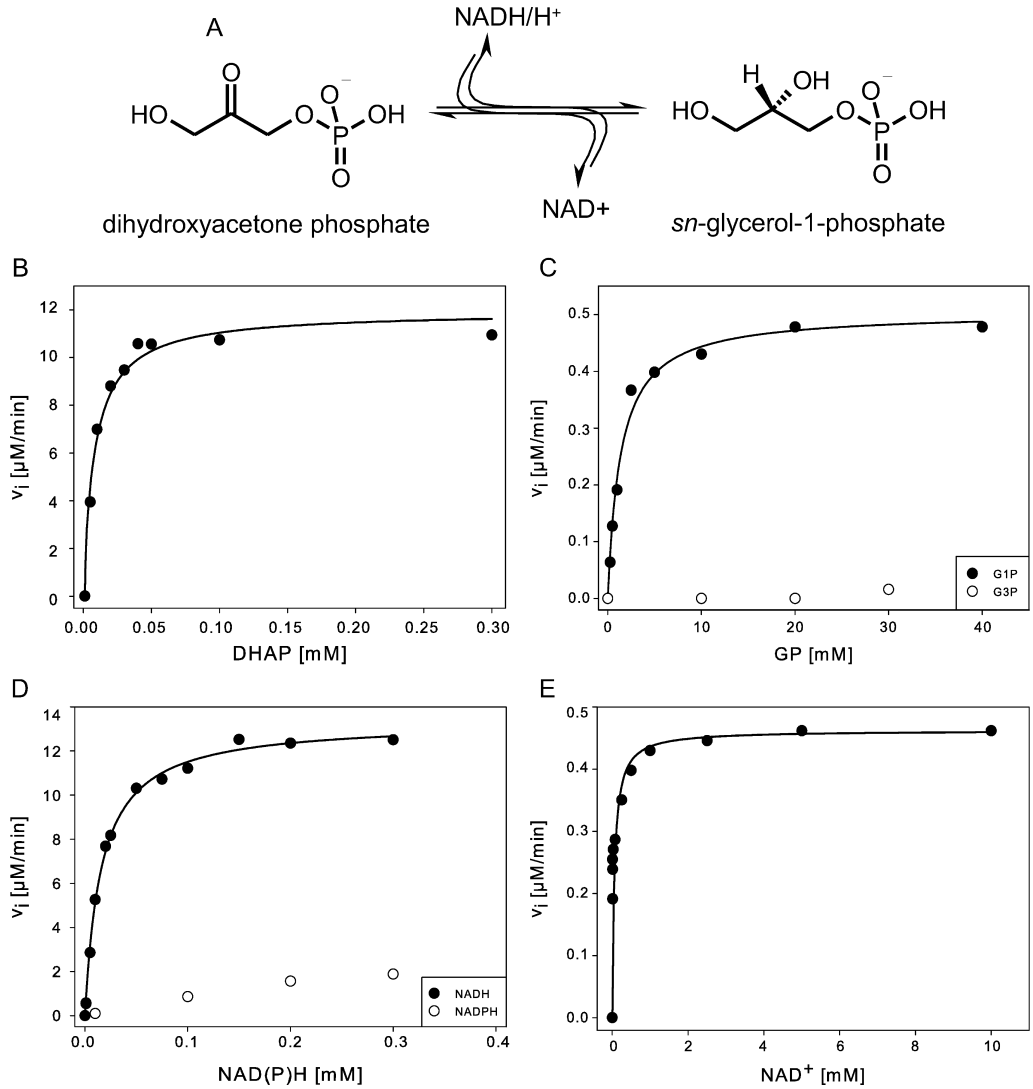

FIGURE 3: Steady-state kinetic measurements of the G1PDH activity of AraM. (A) Scheme of the reversible G1PDH reaction. Saturation curves for (B) DHAP, (C) GP (G1P or G3P), (D) NADH and NADPH, and (E) NAD^+. The measurements were performed in 50 mM Tris-HCl, pH 8.2, 45 °C, in the presence of saturating concentrations of the second substrate ([S] > $10K_M$). The solid lines show the graphs of the Michaelis−Menton equation fitted to the data points.

Table 1: Steady-State Kinetic Constants of the G1PDH Activity of AraM[a]

substrate	K_M (μM)	k_{cat} (min^{-1})	k_{cat}/K_M (min^{-1} μM^{-1})
DHAP	8.1 ± 1.5	11.9 ± 0.50	1.47 ± 0.28
NADH	16.0 ± 0.9	13.3 ± 0.17	0.83 ± 0.05
NADPH	not determined[b]	not determined[b]	$6.5 \times 10^{-3} \pm 1.6 \times 10^{-3}$
G1P	1370 ± 160	0.50 ± 0.01	$3.6 \times 10^{-4} \pm 4.4 \times 10^{-5}$
NAD^+	59.3 ± 3.0	0.46 ± 0.10	$7.8 \times 10^{-3} \pm 1.7 \times 10^{-3}$

[a] Conditions: 50 mM Tris-HCl, pH 8.2, 45 °C, 1 μM (subunit concentration) AraM. The shown values are the mean and standard deviation of three independent measurements in the presence of saturating concentrations of the second substrate (forward reaction: 0.25 mM NADH or 0.1 mM DHAP; reverse reaction: 4 mM NAD^+ or 10 mM G1P). [b] K_M and k_{cat} could not be determined separately due to the high NADPH absorbance at the concentrations necessary for saturation. Therefore, only k_{cat}/K_M^{NADPH} could be calculated from the slope of the linear part of the saturation curve, where [NADPH] ≪ K_M^{NADPH}.

Table 2: Dependence of AraM G1PDH Activity on Supplement with Bivalent Metals to the Growth Medium

supplemented cation	G1PDH activity[b]
−	−
all[a]	+
all except Ni^{2+}	−
Zn^{2+}	−
Ni^{2+}, Zn^{2+}	+
Ni^{2+}	+

[a] Cells for production of recombinant AraM were grown in medium supplemented with a mixture of bivalent cations (1 mM $NiCl_2$, $ZnCl_2$, $CuCl_2$, $CaCl_2$, $MgCl_2$, $MnCl_2$, and $FeCl_2$). [b] (+) Substrate turnover of purified AraM was at least 95% of the fully active protein; (−) substrate turnover of purified AraM was below 5% of the fully active protein.

metal ions. Highly active AraM preparations were obtained only when the growth medium was supplemented with Ni^{2+}, whereas the addition of Zn^{2+} and the other assayed metals did not lead to significant catalytic activity (Table 2). On the basis of these findings, we grew all expression cultures in the presence of 1 mM $NiCl_2$, which reproducibly yielded AraM with high catalytic activity (defined as 100%). This protein was used for the steady-state kinetic experiments documented in Figure 3B−E, as well as for metal-induced reactivation experiments. To this end, residually bound bivalent cations were removed by dialysis against buffer containing 50 mM EDTA, yielding AraM without detectable G1PDH activity. The fluorescence emission and far-UV CD spectra of the protein were identical to those of untreated AraM, suggesting that the absence of catalytic activity was

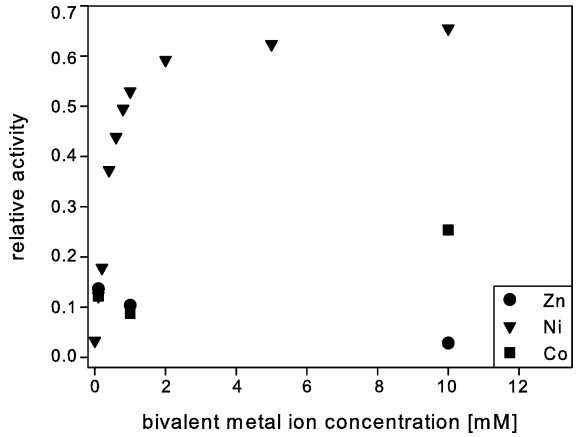

FIGURE 4: Metal-dependent reactivation of AraM following treatment with EDTA. For the sake of clarity, only the data for Ni^{2+}, Zn^{2+}, and Co^{2+} are shown. The activating effect of all other tested bivalent cations (listed in the Experimental Procedures section) was below that of Co^{2+}. The activity measurements were performed in 50 mM Tris-HCl, pH 8.2 at 45 °C, containing 1 μM AraM (subunit concentration), 0.25 mM NADH, and 0.1 mM DHAP. The relative activities refer to purified untreated AraM that was assayed at identical conditions.

not due to denaturation of the polypeptide chain (data not shown). The enzyme was then titrated with different bivalent metal ions, followed by measurements of the G1PDH reaction in the presence of saturating concentrations of both DHAP and NADH. The results of the reactivation experiments are shown in Figure 4. Upon addition of Ni^{2+}, 65% of the activity of untreated AraM could be recovered. In contrast, with all other metals including Zn^{2+}, no more than 25% reactivation was achieved. These findings suggest that Ni^{2+} is the native metal cofactor of AraM, in accordance with our observations that fully active protein could only be obtained when Ni^{2+} was present in the growth medium (Table 2). Moreover, although ICP-OES measurements detected Zn^{2+} at a constant basal concentration in all protein preparations, significantly elevated amounts of Ni^{2+} were only found in preparations with high G1PDH activity (data not shown). While Zn^{2+} is usually in tetrahedral coordination, Ni^{2+} is coordinated hexagonally. We are planning to solve the crystal structure of AraM to reveal how the metal ion is coordinated in the active site and to understand why the Zn^{2+} is replaced by Ni^{2+} in this protein.

Phylogenetic Distribution of AraM and Related Proteins. AraM from *B. subtilis* is the first G1PDH to be identified within a bacterial species. G1PDHs belong to the class of proteins with a dehydroquinate synthase-like fold, as defined in the SCOP (Structural Classification of Proteins) database (*36*). Structurally and functionally related proteins are the dehydroquinate synthases (DHQS), alcohol dehydrogenases (ADH), and glycerol dehydrogenases (GDH). However, G1PDHs show no significant sequence similarity to G3PDHs (*7*). To analyze the species distribution of AraM, we searched the NCBI nr database for similar sequences, constructed a multiple alignment, and calculated a phylogenetic tree (Supporting Information Figure 2).

Whereas proteins with a DHQS-like fold are ubiquitously present in bacteria, we found AraM-like proteins only in a subset of them, which nevertheless contains quite diverse species. This has previously been explained by independent horizontal gene transfer (HGT) events of the G1PDH gene from archaea to bacteria, as such patchy distributions are indicative of HGT (*25*). A possible role for AraM-produced G1P in bacteria is not obvious from existing knowledge, as it has not been identified as a free metabolite in bacterial cells until now. As a consequence, without any evolutionary pressure, a G1PDH gene obtained by HGT would soon get lost or at least suffer from a decline in catalytic efficiency by accumulating mutations. However, AraM is highly active, suggesting that it has an important function in *B. subtilis* and other bacteria. Interestingly, an AraM homologue also exists in Rickettsiales (Gram-negative α-proteobacteria). These intracellular parasites abandoned many biosynthetic pathways and thus belong to the species with the smallest genomes known (about 1 Mbp, 800−900 ORFs; *37*). The finding that an AraM-like protein is encoded in their genomes further supports our conclusion that it has developed a crucial function in bacteria after it had been acquired from archaea by HGT.

Putative Physiological Function of AraM. To gain insight into the metabolic role of AraM, we generated an *araM* knockout mutant by insertional mutagenesis. Compared to wt, the knockout strain exhibited an approximately 30% slower growth on different media (CSE, LB). A similar phenotype has been observed for a large scale deletion within the *ara* operon including *araM* (*14*). To test whether AraM acts as G1PDH activity *in vivo*, we grew wt and knockout strains on C minimal medium supplemented with G1P (50 mM) as the sole carbon source. While the knockout cells could not thrive on this medium, the wt culture showed moderate growth, resulting in an $OD_{600} \sim 1.2$ when incubated overnight at 37 °C. We conclude that via the G1PDH back-reaction, AraM oxidizes G1P to DHAP, which is then channelled into glycolysis.

Is the native function of AraM to make G1P available as an energy source? Several lines of evidence make this possibility appear unlikely. *B. subtilis* is a saprophyte soil bacterium that lives on rotting plant material. This substrate contains many different sugars and proteins, which can be made available by a large variety of degradation enzymes encoded in the *B. subtilis* genome. In contrast, the occurrence of G1P in plant material has not been described, and thus it is unlikely that it is a relevant nutrient in the natural habitat of *B. subtilis*. Furthermore, the high K_M of the AraM back-reaction ($K_M^{G1P} = 1.4$ mM; cf. Table 1) argues against the usage of G1P as a carbon source. For these reasons, we rather propose an anabolic function of AraM, like the G1PDHs have in archaea.

When searching the literature for a putative G1P-involving biosynthetic pathway in bacteria, we came across the PcrB protein, whose X-ray structure has been solved recently (*38*). PcrB occurs in Gram-positive bacteria like *Bacillus*, *Streptococcus*, *Listerium*, or *Chlorobium* and is structurally similar to the archaeal geranylgeranylglyceryl phosphate synthase (GGGPS). GGGPS converts G1P and geranylgeranyl pyrophosphate (GGPP) to GGGP, a precursor of the archaeal membrane lipids, and thus catalyzes a reaction that has no biological significance in bacteria. Since, however, the G1P complexing residues are completely conserved in PcrB (*4*), it seems likely that the enzyme turns over AraM-generated G1P together with a second yet unidentified substrate. Payandeh et al. (*4*) discuss a possible involvement of PcrB in the biosynthesis of lipoteichoic acids (LTA), a cell wall

component of Gram-positive bacteria. LTA are composed of a glycolipid anchor and a poly(G1P) tail, which is synthesized from phosphatidylglycerol molecules by the repetitive transfer of G3P units, which are isomerized to G1P upon their addition to the growing chain (*11, 39*). Whether the poly(G1P) tail is synthesized directly on the glycolipid anchor or assembled separately and then transferred is not fully understood. It has been suggested, however, that a specific enzyme transfers the first G1P unit via an unknown mechanism to the glycolipid anchor, followed by the addition of the remainder of the poly(G1P) tail (*11*). We suspected that this unknown protein might be PcrB, which uses G1P delivered by AraM. To test this hypothesis, we quantified the LTA content in the AraM knockout mutant by ELISA, assuming that the lack of G1P might greatly reduce the amount of LTA. However, after overnight growth, no difference in the LTA content could be observed between knockout and wt cells. This finding does not support that AraM-generated G1P is used for the biosynthesis of LTA.

In order to identify the second substrate of PcrB, we modeled a variety of metabolites into the known PcrB crystal structure (*38*). The results confirmed that G1P fits well into the putative active site, whereas the Mg^{2+}-GGPP binding pocket of GGGPS is slightly modified in PcrB. The residues for binding the Mg^{2+}-diphosphate moiety of GGPP are conserved, but the ruler at the other end of the long binding groove that determines the polyprenyl chain length in GGPPS is obviously missing in PcrB. The protein is more open in this region, allowing the binding of indefinitely long hydrophobic chains. Alternatively to polyprenyl chains, a simple alkyl chain might bind as well. On the basis of these findings, we propose that PcrB might act as a prenyl- or alkyltransferase that fuses such a molecule to G1P via an ether bond, yielding a phosphoglycerolipid. This hypothesis will now be further tested experimentally.

ACKNOWLEDGMENT

We thank Christian Vogl and Jürgen Stolz for supplying us with *B. subtilis* cells, Harald Huber for help with the ICP-OES analyses, Helmut Durchschlag for running the analytical ultracentrifuge, Eduard Hochmuth and Rainer Deutzmann for performing the ESI-MS analyses, and Rainer Merkl and Frank Raushel for critical reading of the manuscript.

SUPPORTING INFORMATION AVAILABLE

Product inhibition of AraM activity by G1P and detailed discussion of the phylogenetic analysis of AraM and related protein sequences. This material is available free of charge via the Internet at http://pubs.acs.org.

REFERENCES

1. Woese, C. R., Kandler, O., and Wheelis, M. L. (1990) Towards a natural system of organisms: proposal for the domains Archaea, Bacteria, and Eucarya. *Proc. Natl. Acad. Sci. U.S.A. 87*, 4576–4579.
2. Wächtershäuser, G. (2003) From pre-cells to Eukarya—a tale of two lipids. *Mol. Microbiol. 47*, 13–22.
3. Martin, W., and Russell, M. J. (2003) On the origins of cells: a hypothesis for the evolutionary transitions from abiotic geochemistry to chemoautotrophic prokaryotes, and from prokaryotes to nucleated cells. *Philos. Trans. R. Soc. London, Ser. B: Biol. Sci. 358*, 59–85.
4. Payandeh, J., Fujihashi, M., Gillon, W., and Pai, E. F. (2006) The crystal structure of (S)-3-O-geranylgeranylglyceryl phosphate synthase reveals an ancient fold for an ancient enzyme. *J. Biol. Chem. 281*, 6070–6078.
5. Payandeh, J., and Pai, E. F. (2007) Enzyme-driven speciation: crystallizing Archaea via lipid capture. *J. Mol. Evol. 64*, 364–374.
6. Koga, Y., Kyuragi, T., Nishihara, M., and Sone, N. (1998) Did archaeal and bacterial cells arise independently from noncellular precursors? A hypothesis stating that the advent of membrane phospholipid with enantiomeric glycerophosphate backbones caused the separation of the two lines of descent. *J. Mol. Evol. 46*, 54–63.
7. Daiyasu, H., Hiroike, T., Koga, Y., and Toh, H. (2002) Analysis of membrane stereochemistry with homology modeling of sn-glycerol-1-phosphate dehydrogenase. *Protein Eng. 15*, 987–995.
8. Koga, Y., Ohga, M., Tsujimura, M., Morii, H., and Kawarabayasi, Y. (2006) Identification of sn-glycerol-1-phosphate dehydrogenase activity from genomic information on a hyperthermophilic archaeon *Sulfolobus tokodaii* strain 7. *Biosci., Biotechnol., Biochem. 70*, 282–285.
9. Boucher, Y., Kamekura, M., and Doolittle, W. F. (2004) Origins and evolution of isoprenoid lipid biosynthesis in archaea. *Mol. Microbiol. 52*, 515–527.
10. Taron, D. J., Childs, W. C., III, and Neuhaus, F. C. (1983) Biosynthesis of D-alanyl-lipoteichoic acid: role of diglyceride kinase in the synthesis of phosphatidylglycerol for chain elongation. *J. Bacteriol. 154*, 1110–1116.
11. Neuhaus, F. C., and Baddiley, J. (2003) A continuum of anionic charge: structures and functions of D-alanyl-teichoic acids in gram-positive bacteria. *Microbiol. Mol. Biol. Rev. 67*, 686–723.
12. Itabashi, Y., and Kuksis, A. (1997) Reassessment of stereochemical configuration of natural phosphatidylglycerols by chiral-phase high-performance liquid chromatography and electrospray mass spectrometry. *Anal. Biochem. 254*, 49–56.
13. Perepelov, A. V., Wang, Q., Senchenkova, S. N., Shevelev, S. D., Zhao, G., Shashkov, A. S., Feng, L., Knirel, Y. A., and Wang, L. (2006) Structure of a teichoic acid-like O-polysaccharide of *Escherichia coli* O29. *Carbohydr. Res. 341*, 2176–2180.
14. Sa-Nogueira, I., Nogueira, T. V., Soares, S., and de Lencastre, H. (1997) The *Bacillus subtilis* L-arabinose (*ara*) operon: nucleotide sequence, genetic organization and expression. *Microbiology 143* (Part 3), 957–969.
15. Pace, C. N., Vajdos, F., Fee, L., Grimsley, G., and Gray, T. (1995) How to measure and predict the molar absorption coefficient of a protein. *Protein Sci. 4*, 2411–2423.
16. Yphantis, D. A. (1964) Equilibrium ultracentrifugation of dilute solutions. *Biochemistry 3*, 297–317.
17. Durchschlag, H. (1986) Specific volumes of biological macromolecules and some other molecules of biological interest in *Thermodynamic Data for Biochemistry and Biotechnology* (Hinz, H.-J., Ed.) pp 45−128, Springer, Berlin.
18. Cohn, E. J., and Edsall, J. T. (1943) *Proteins, amino acids and peptides as ions and dipolar ions*, Reinhold, New York.
19. Stoll, V. S., and Blanchard, J. S. (1990) Buffers: principles and practice. *Methods Enzymol. 182*, 24–38.
20. Reinstein, J., Vetter, I. R., Schlichting, I., Rosch, P., Wittinghofer, A., and Goody, R. S. (1990) Fluorescence and NMR investigations on the ligand binding properties of adenylate kinases. *Biochemistry 29*, 7440–7450.
21. Vagner, V., Dervyn, E., and Ehrlich, S. D. (1998) A vector for systematic gene inactivation in *Bacillus subtilis*. *Microbiology 144* (Part 11), 3097–3104.
22. Martin-Verstraete, I., Debarbouille, M., Klier, A., and Rapoport, G. (1990) Levanase operon of *Bacillus subtilis* includes a fructose-specific phosphotransferase system regulating the expression of the operon. *J. Mol. Biol. 214*, 657–671.
23. Fedtke, I., Mader, D., Kohler, T., Moll, H., Nicholson, G., Biswas, R., Henseler, K., Gotz, F., Zahringer, U., and Peschel, A. (2007) A *Staphylococcus aureus* ypfP mutant with strongly reduced lipoteichoic acid (LTA) content: LTA governs bacterial surface properties and autolysin activity. *Mol. Microbiol. 65*, 1078–1091.
24. Altschul, S. F., Madden, T. L., Schaffer, A. A., Zhang, J., Zhang, Z., Miller, W., and Lipman, D. J. (1997) Gapped BLAST and PSI-BLAST: a new generation of protein database search programs. *Nucleic Acids Res. 25*, 3389–3402.
25. Pereto, J., Lopez-Garcia, P., and Moreira, D. (2004) Ancestral lipid biosynthesis and early membrane evolution. *Trends Biochem. Sci. 29*, 469–477.

26. Han, J. S., Kosugi, Y., Ishida, H., and Ishikawa, K. (2002) Kinetic study of sn-glycerol-1-phosphate dehydrogenase from the aerobic hyperthermophilic archaeon *Aeropyrum pernix* K1. *Eur. J. Biochem. 269*, 969–976.
27. Nishihara, M., and Koga, Y. (1997) Purification and properties of sn-glycerol-1-phosphate dehydrogenase from *Methanobacterium thermoautotrophicum*: characterization of the biosynthetic enzyme for the enantiomeric glycerophosphate backbone of ether polar lipids of Archaea. *J. Biochem. (Tokyo) 122*, 572–576.
28. Vishwasrao, H. D., Heikal, A. A., Kasischke, K. A., and Webb, W. W. (2005) Conformational dependence of intracellular NADH on metabolic state revealed by associated fluorescence anisotropy. *J. Biol. Chem. 280*, 25119–25126.
29. von Ellenrieder, G., Kirschner, K., and Schuster, I. (1972) The binding of oxidized and reduced nicotinamide adenine-dinucleotide to yeast glyceraldehyde-3-phosphate dehydrogenase. *Eur. J. Biochem. 26*, 220–236.
30. Fjeld, C. C., Birdsong, W. T., and Goodman, R. H. (2003) Differential binding of NAD^+ and NADH allows the transcriptional corepressor carboxyl-terminal binding protein to serve as a metabolic sensor. *Proc. Natl. Acad. Sci. U.S.A. 100*, 9202–9207.
31. Wolff, E. C., Wolff, J., and Park, M. H. (2000) Deoxyhypusine synthase generates and uses bound NADH in a transient hydride transfer mechanism. *J. Biol. Chem. 275*, 9170–9177.
32. Bando, M., Oka, M., Kawai, K., Obazawa, H., Kobayashi, S., and Takehana, M. (2006) NADH binding properties of rabbit lens lambda-crystallin. *Mol. Vision 12*, 692–697.
33. Tatusov, R. L., Natale, D. A., Garkavtsev, I. V., Tatusova, T. A., Shankavaram, U. T., Rao, B. S., Kiryutin, B., Galperin, M. Y., Fedorova, N. D., and Koonin, E. V. (2001) The COG database: new developments in phylogenetic classification of proteins from complete genomes. *Nucleic Acids Res. 29*, 22–28.
34. Han, J. S., and Ishikawa, K. (2005) Active site of Zn(2+)-dependent sn-glycerol-1-phosphate dehydrogenase from *Aeropyrum pernix* K1. *Archaea 1*, 311–317.
35. Ruzheinikov, S. N., Burke, J., Sedelnikova, S., Baker, P. J., Taylor, R., Bullough, P. A., Muir, N. M., Gore, M. G., and Rice, D. W. (2001) Glycerol dehydrogenase. structure, specificity, and mechanism of a family III polyol dehydrogenase. *Structure 9*, 789–802.
36. Andreeva, A., Howorth, D., Brenner, S. E., Hubbard, T. J., Chothia, C., and Murzin, A. G. (2004) SCOP database in 2004: refinements integrate structure and sequence family data. *Nucleic Acids Res. 32*, D226–D229.
37. Andersson, S. G., Zomorodipour, A., Andersson, J. O., Sicheritz-Ponten, T., Alsmark, U. C., Podowski, R. M., Naslund, A. K., Eriksson, A. S., Winkler, H. H., and Kurland, C. G. (1998) The genome sequence of *Rickettsia prowazekii* and the origin of mitochondria. *Nature 396*, 133–140.
38. Badger, J., Sauder, J. M., Adams, J. M., Antonysamy, S., Bain, K., Bergseid, M. G., Buchanan, S. G., Buchanan, M. D., Batiyenko, Y., Christopher, J. A., Emtage, S., Eroshkina, A., Feil, I., Furlong, E. B., Gajiwala, K. S., Gao, X., He, D., Hendle, J., Huber, A., Hoda, K., Kearins, P., Kissinger, C., Laubert, B., Lewis, H. A., Lin, J., Loomis, K., Lorimer, D., Louie, G., Maletic, M., Marsh, C. D., Miller, I., Molinari, J., MullerDieckmann, H. J., Newman, J. M., Noland, B. W., Pagarigan, B., Park, F., Peat, T. S., Post, K. W., Radojicic, S., Ramos, A., Romero, R., Rutter, M. E., Sanderson, W. E., Schwinn, K. D., Tresser, J., Winhoven, J., Wright, T. A., Wu, L., Xu, J., and Harris, T. J. (2005) Structural analysis of a set of proteins resulting from a bacterial genomics project. *Proteins 60*, 787–796.
39. Roethlisberger, P., Iida-Tanaka, N., Hollemeyer, K., Heinzle, E., Ishizuka, I., and Fischer, W. (2000) Unique poly(glycerophosphate) lipoteichoic acid and the glycolipids of a *Streptococcus* sp. closely related to *Streptococcus pneumoniae*. *Eur. J. Biochem. 267*, 5520–5530.

BI8005779